Enskog-Vlasov Simulations in High Pressure Environments

R. Tietz*[1], R. Stierle[2], F. Fasoulas[1], M. Pfeiffer[1]
[1]Institute of Space Systems, University of Stuttgart, Germany
[2]Institute of Thermodynamics and Thermal Process Engineering, University of Stuttgart, Germany
*Corresponding author: rtietz@irs.uni-stuttgart.de

Introduction

The climate crisis is one of the most challenging issues facing our society. Global carbon dioxide emissions must therefore be significantly reduced. One of the sectors with the least savings is transportation. Therefore, internal combustion engines must be replaced by electric alternatives, but where this is not possible, combustion must be made more efficient. This would reduce emissions (including soot) and conserve valuable fuels.
One idea by Lamanna et al. [8] is to improve the mixing of fuel with air. At present, small droplets of fuel are dispersed in the air during combustion, creating oxygen and fuel rich areas in the combustion chamber, which reduces efficiency. If the fuel is heated above its critical temperature, the liquid fuel droplets become supercritical and the mixing problem would become much simpler and more efficient through single phase mixing. Lamanna et al. have also developed a model that estimates the time it takes for the droplet to become supercritical [8]. However, this model relies on data on evaporation coefficients at such conditions (near critical and high pressure), which are not available. To fill this gap, evaporation simulations are carried out at such conditions to extract the evaporation coefficients at the end.
In this work, such simulations have been performed with a particle-based statistical Enskog-Vlasov solver containing two species. A primary liquid species (argon) and a second species (neon) to apply the high pressure to the liquid. So far, only multi-species Enskog-Vlasov [5] solvers have been presented, which vary the strength of the intermolecular attraction potential of the different species [10, 6] but not their diameter, which is done in this work.

Numerical Modelling

The simulations are performed by an adapted Direct Simulation Monte Carlo [3] algorithm, which performs statistical particle simulations, where each particle represents a number of physical atoms. The behavior of the particles is simulated by statistical assumptions, which greatly reduces the computational effort compared to deterministic simulations such as Molecular Dynamics [7]. Statistical means that for different events (such as collisions) a probability is calculated and a random number determines whether the event takes place or not. In addition, random numbers determine the outcome of the event.
A schematic of the solver can be seen in Figure 1, which consists of several mostly decoupled steps, as movement of and collisions between the particles. At the beginning of each simulation the simulation is *initialized*, and the computational domain is populated with the simulation particles. Afterwards the time step loop starts, until the simulations ends. The first stage in this loop is the *field solver*, which determines the number density in each element and convolutes it with the derivative of the Sutherland potential to obtain the force onto the particles in every element. This force is used in the *particle movement* step to compute the new particle velocities and positions with a low storage explicit Runge-Kutta 3rd order. Subsequently, in the *boundary* step all particle paths are checked for intersections with boundaries and their conditions are applied to them.
In the *pairing* stage, the required number of particle pairs in each element for each species is generated: $N_{pairs} = \frac{1}{2} N P_{max}$, where N is the number of particles in the element and P_{max} is an estimate of the maximum collision probability based on the last time steps. For each pair,

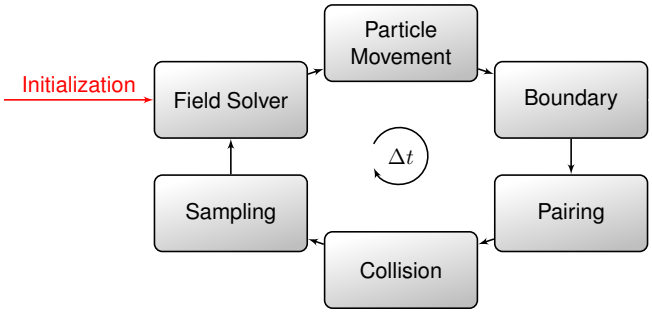

Figure 1. Schematic of the solver

the first particle is randomly selected and a random unit vector $\vec{k}$ is drawn. The second particle is the closest particle of the assigned species of the pair, located the mean diameter away from the first particle in the direction of $\vec{k}$. In the *collision* step, the equilibrium pair correlation function Y is evaluated, which incorporates the effects of the radial distribution function. Y is based on BMCSL equation of state [4] is evaluated for all pairs. This information is used to calculate the collision probability:

$$P = R\left(\left\langle \vec{c}_\mathrm{r} \cdot \vec{k} \right\rangle\right) \frac{4\pi d_{ij}^2}{\omega_k} Y\left(\vec{x} + \frac{d_i \vec{k}}{2}, i, j\right) n_{2,j} \Delta t \tag{1}$$

This collision probability is normalized by P_{max} and compared to a random number evenly distributed between zero and one. If the random number is lower, then the collision occurs and the particle velocities are updated by: $v_i' = v_i \pm 2\frac{m_i}{m_i+m_j} < \vec{c}_\mathrm{r} \cdot \vec{k} > \vec{k}$. In the final step *sampling* the particle properties are averaged to calculate the macroscopic moments as density n, bulk velocity u and temperature T.

Simulation Setup

The evaporation simulations were performed with an argon-neon mixture, where neon is in a supercritical state. To determine the molecular parameter, the strength of the attractive potential ϕ_d was fitted to critical temperature data. The molecular diameter for argon was fitted to equilibrium density simulations of SAFT-VR Mie [1, 2] simulations, while that of neon was fitted to pressure data [9]. The simulations were performed at three different temperature levels: $0.663T_{c,\mathrm{Ar}}$, $0.767T_{c,\mathrm{Ar}}$ and $0.9T_{c,\mathrm{Ar}}$. This gives the following parameters:

Table 1. Molecular properties of the simulations

	ϕ_d	$d(T = 0.663T_{c,\mathrm{Ar}})$	$d(T = 0.767T_{c,\mathrm{Ar}})$	$d(T = 0.9T_{c,\mathrm{Ar}})$
Ar	$2.759 \cdot 10^{-21}$ J	$3.332 \cdot 10^{-10}$ m	$3.227 \cdot 10^{-10}$ m	$3.142 \cdot 10^{-10}$ m
Ne	$8.136 \cdot 10^{-22}$ J	$2.590 \cdot 10^{-10}$ m	$2.566 \cdot 10^{-10}$ m	$2.549 \cdot 10^{-10}$ m

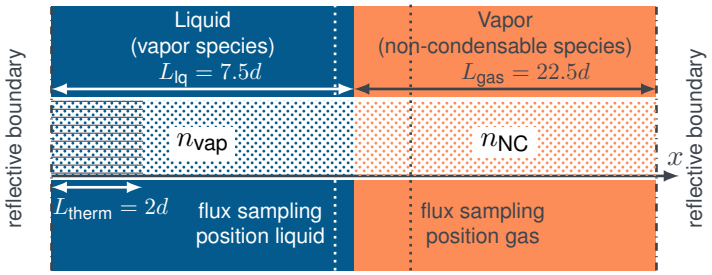

Figure 2. Initial condition of the simulations

The computational domain is an enclosed space of 30 cross-sectional diameter of argon and is depicted in Figure 2. A thermostat is required to maintain a stable temperature to counteract evaporation heat losses.

Results and Discussion

The results of the simulations are shown in Figure 3. It can be seen that at higher pressure and lower temperature more neon is dissolved in the liquid phase. In addition, more neon accumulates at the liquid-vapor interface. This accumulation can also be seen in other evaporation results [10]. With increasing pressure, the argon density in the vapor also increases.

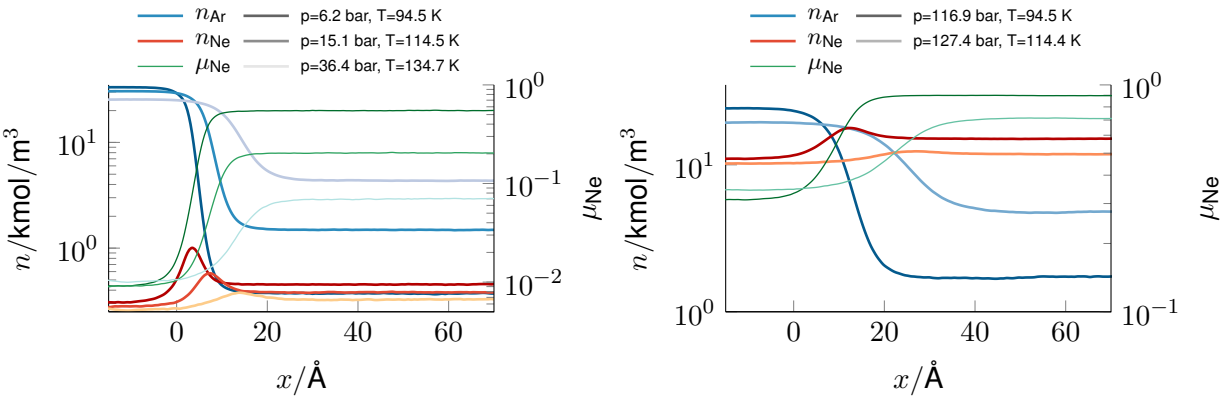

(a) Low pressure cases

(b) High pressure cases

Figure 3. number density profiles of the simulations

The mole fractions in the liquid and vapor regions were extracted and compared with the SAFT-VRQ Mie results [1, 2], which are shown in Figure 4. They show the same trend, but at higher pressures and temperatures the deviations are greater. This may be due to the use of different interaction potentials.

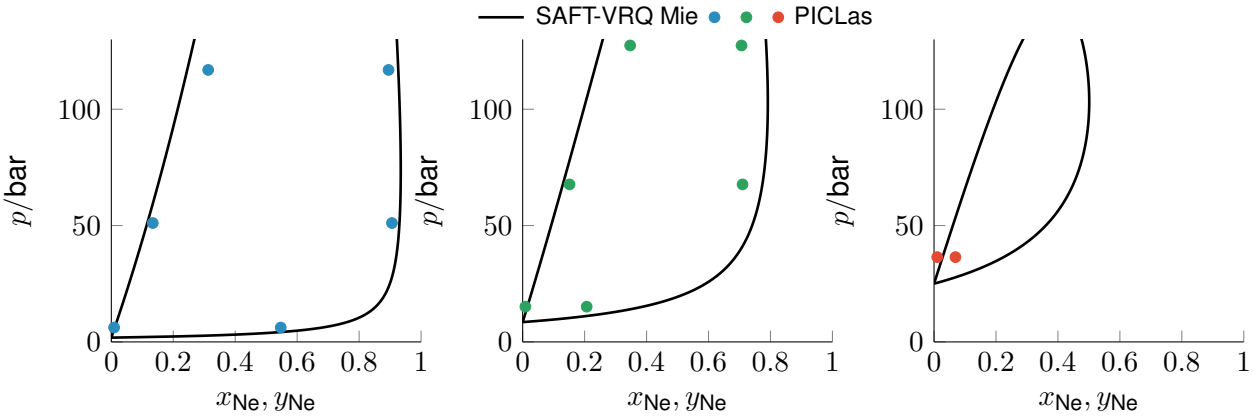

(a) $T/T_c = 0.633$

(b) $T/T_c = 0.767$

(c) $T/T_c = 0.900$

Figure 4. Enskog-Vlasov result compared to SAFT-VRQ Mie[1, 2]

Conclusion

This work briefly introduces a novel multi-species solver for the Enskog-Vlasov equation, which is able to simulate liquid vapor profiles of a binary mixture. The bulk vapour and liquid states are in good agreement with SAFT-VRQ Mie results.

The next steps are to perform further simulations of more application-like cases. From these simulations the evaporation coefficients can be sampled and fed into the Lamanna et al. model.

Nomenclature

Ar	argon [-]	t	time [s]
c_r	relative velocity [m/s]	T	temperature [K]
d	molecular diameter [m]	T_c	critical temperature [K]
i	Species [-]	$\vec{u}$	bulk velocity [m/s]
j	2nd Species [-]	$\vec{v}$	particle velocity [m/s]
$\vec{k}$	collision vector [-]	x	mole fraction in liquid [-]
m	molecular mass [kg]	y	mole fraction in vapor [-]
n	particle density [1/m^3]	$Y()$	equilibrium pair correlation function [-]
n_2	particle density in 2nd element [1/m^3]	Δt	time step length [s]
Ne	neon [-]	π	3.14159... [-]
p	pressure [bar]	ϕ_d	Sutherland potential strength at a distance of d [J]
P	collision probability [-]		
P_{max}	maximum collision probability [-]	ω_k	statistical particle weight [-]
		μ	mole fraction [-]

References

[1] A. Aasen, M. Hammer, Å. Ervik, E. A. Müller, and Ø. Wilhelmsen. *The Journal of Chemical Physics*, 151(6), 2019.

[2] A. Aasen, M. Hammer, E. A. Müller, and Ø. Wilhelmsen. *The Journal of Chemical Physics*, 152(7), 2020.

[3] G. A. Bird. *Molecular Gas Dynamics and Direct Simulation of Gas Flows*. Oxford Science Publications 42, 1994.

[4] T. Boublík. *The Journal of chemical physics*, 53(1):471–472, 1970.

[5] D. Enskog. *Kinetische Theorie der Wärmeleitung: Reibung und Selbst-diffusion in Gewissen verdichteten gasen und flüssigkeiten*. Almqvist & Wiksells boktryckeri-a.-b., 1922.

[6] A. Frezzotti, L. Gibelli, D. A. Lockerby, and J. E. Sprittles. *Physical Review Fluids*, 3(5):054001, 2018.

[7] A. Frezzotti, L. Gibelli, and S. Lorenzani. *Physics of Fluids*, 17(1), 2005.

[8] B. W. G. Lamanna, C. Steinhausen. On the role of transcritical evaporation in controlling the transition from two-phase to single-phase mixing. *32nd International Conference on Liquid Atomization and Spray Systems, Naples*, 2023.

[9] P. Linstrom and E. W.G. Mallard. *NIST Chemistry WebBook, NIST Standard Reference Database Number 69*. National Institute of Standards and Technology, 2024.

[10] K. Ohashi, K. Kobayashi, H. Fujii, and M. Watanabe. *Scientific Reports*, 10(1):8143, 2020.